To appear in the *Journal of Geophysical Research*, 1997.

Alfvénic fluctuations in fast and slow solar winds

S. Orlando,[1] Y.-Q. Lou,[2] G. Peres,[1] and R. Rosner[2]

Abstract

We compute properties of Alfvénic fluctuations within a wide frequency range (i.e., $10^{-6}\ \mathrm{s}^{-1} \lesssim f \lesssim 10^{-2}\ \mathrm{s}^{-1}$) in both high– and low–speed magnetized radial solar winds. In particular, the radial and frequency variations of the normalized cross helicity σ_c, the Alfvén ratio $\mathcal{R}_A$, and other relevant quantities associated with Alfvénic fluctuations are presented and analyzed. Because of the existence of the Alfvén critical radius r_A and a characteristic frequency f_c for a given magnetized solar wind profile, continuous reflection effects are clearly manifest at frequencies lower than several times f_c. Since outward propagating fluctuations which many authors consider Alfvénic fluctuations have been detected in the high–latitude solar wind (which is fast and steady), such continuous reflection effects in the low–frequency end of the fluctuation spectrum may be found in the Ulysses data. In order to strengthen our case, comparisons are carried out between our theoretical results and previous data analyses of observations from the Helios 1 and 2 spacecraft in the radial range of $0.29\ \mathrm{AU} \lesssim r \lesssim 1.0\ \mathrm{AU}$. Stronger evidence for continuous reflection effects of low–frequency Alfvénic fluctuations is found in the high–speed solar wind close to the Sun than in the low–speed solar wind in general.

1. Introduction

In situ experiments aboard Ulysses spacecraft have revealed several important facts about the solar wind at high heliographic latitudes a few AU away from the Sun, namely, (1) the average solar wind properties are remarkably stable, and the radial wind speed U_R ($\gtrsim 700\ \mathrm{km\ s}^{-1}$) is persistently fast [*Phillips et al.*, 1995; *Geiss et al.*, 1995; *Grall et al.*, 1996]; (2) the radial magnetic flux A_B in the wind does not vary appreciably with latitude [*Smith et al.*, 1995b; *Balogh et al.*, 1995], so that the radial magnetic field B scales as $\sim r^{-2}$ over the polar heliosphere [*Lou*, 1993a]; and (3) large–amplitude transverse magnetic field fluctuations associated with outgoing Alfvén waves overwhelm the radial magnetic field B in the polar solar wind [*Balogh et al.*, 1995; *Jokipii and Kóta*, 1989; *Lou*, 1992a, b].

Implications of these basic facts and of other important findings from Ulysses particle and cosmic ray experiments [*Lanzerotti et al.*, 1995; *Keppler et al.*, 1995; *Simpson et al.*, 1995] are broad regarding various dynamic processes occurring in the three–dimensional heliosphere [*Lou*, 1996]. For example, the role of magnetic stress in producing the high–speed polar solar wind needs to be pursued further [*Smith et al.*, 1995a], especially in view of the detection of large–amplitude transverse magnetic field fluctuations associated with outward propagating Alfvén waves in the fast polar solar wind [*Orlando et al.*, 1996].

The main purpose of this paper is to calculate specifically the radial and frequency dependences of the normalized cross helicity σ_c, the Alfvén ratio $\mathcal{R}_A$, and other relevant quantities associated with Alfvénic fluctuations in the fast polar solar wind using the theoretical model framework of *Lou* [1993a] for Alfvénic fluctuations in a magnetized radial wind profile. We expect that as a result of the presence of the Alfvén critical point r_A and a characteristic frequency f_c for a given magnetized solar wind profile [*Heinemann and Olbert*, 1980; *Lou*, 1993a], continuous reflection effects of Alfvénic fluctuations appear conspicuously at frequencies lower than several times f_c. These theoretical predictions can be further tested by frequency spectral analysis of Ulysses data for polar solar wind fluctuations over sufficiently long timescales [*Smith et al.*, 1995b; *Balogh et al.*, 1995].

The primary reason we emphasize the application of our model analysis to Alfvénic fluctuations in the polar solar wind is that the mean polar wind can be well approximated as a spherically symmetric radial wind within a large solid angle [*Lou*, 1993a]. In principle, our theoretical results should be equally applicable in the inner equatorial solar wind (i.e., $r \lesssim 1$ AU) where the azimuthal magnetic field becomes weak close to the Sun, although the presence of alternating fast and slow wind streams considerably complicates the detection of the effect we are studying. With these precautions in mind we proceed to compare our theoretical results in both fast and slow solar winds with previous data analyses [*Bruno et al.*, 1985; *Roberts et al.*, 1987b; *Marsch and Tu*, 1990] of observations from the Helios 1 and 2 spacecraft. We find stronger evidence for continuous reflection effects of low–frequency Alfvénic fluctuations in the high–speed solar wind close to the Sun than in the low–speed solar wind in general. We regard this as an encouragement to further test our theoretical results with the Ulysses data.

On the theoretical side, there exist two different yet complementary perspectives with regard to the nature of interplanetary fluctuations. These are that such fluctuations are due to (1) turbulence [*Coleman*, 1968; *Barnes*, 1979; *Zhou and Matthaeus*, 1990; *Roberts and Goldstein*, 1991; *Tu and Marsch*, 1995; *Goldstein et al.*, 1995] or (2) magnetohydrodynamic (MHD) waves [*Belcher et al.*, 1969; *Belcher and Davis*, 1971; *Hollweg*, 1978; *Bavassano and Smith*, 1986; *Roberts et al.*, 1987a, b; *Lou*, 1993a, b, 1994; *Smith et al.*, 1995b; *Balogh et al.*, 1995]. Both aspects manifest themselves in solar wind fluctuations under various conditions; in fact, so–called two–component models of solar wind fluctuations take both convective turbulence and MHD waves into account [*Matthaeus et al.*, 1990; *Marsch and Tu*, 1993; *Tu and Marsch*, 1993; *Lou*, 1995]. In this broader context the present paper emphasizes low–frequency reflection effects of Alfvénic fluctuations in fast–stream solar wind close to the Sun and in the fast polar solar wind. We caution, however, that the simplifying geometric assumptions made in this paper (in particular the assumption of spherical symmetry) make the application of our results to solar wind flows very close to the Sun (e.g., $\lesssim 0.3$ AU) somewhat questionable; near the Sun, the solar magnetic field is geometrically highly complex, and the solar wind outflows far from spherically symmetric, even at the poles [*Munro and Jackson*, 1977; *Holzer*, 1977].

This paper is structured as follows. In section 2 we describe the parametric form of the background solar wind profile and the equations for Alfvénic fluctuations in such a wind. In section 3 we present and analyze the frequency and radial variations of the normalized cross helicity σ_c and the Alfvén ratio $\mathcal{R}_A$ in the fast polar solar wind. In section 4 we use the data from the Helios 1 and 2 spacecraft to fit both fast– and slow–speed solar wind profiles and to compare Alfvénic fluctuations properties with results of previous data analyses. In section 5 we present the final discussion and summary.

2. Theoretical Model Formulation

Since the mean solar wind properties at high heliographic latitudes (i.e., $\gtrsim \pm 35^\circ$) are remarkably stable [*Phillips et al.*, 1995] and since the radial magnetic flux $r^2B(r) = A_B$ does not vary appreciably with latitude [*Smith et al.*, 1995b], a spherically symmetric model [*Lou*, 1993a] of a magnetized radial solar wind as applied to the polar heliosphere within a fairly large solid angle ($\lesssim \pi/2$ sr) is a fairly good approximation. In the linear regime the propagation of three–dimensional transverse incompressible Alfvénic fluctuations decouples from the propagation of three–dimensional compressible MHD fast and slow waves in such a background radial wind [*Lou*, 1993b]. For Alfvén waves which involve perturbations of transverse magnetic field $\mathbf{b}_\perp \equiv (0, b_\theta, b_\phi)$ and transverse velocity $\mathbf{v}_\perp \equiv (0, v_\theta, v_\phi)$ the relevant equations in the spherical polar coordinate system (r, θ, ϕ) are

$$\frac{\partial j}{\partial t} = \frac{1}{r^2}\frac{\partial}{\partial r}(r^2 B\xi) - \frac{1}{r^2}\frac{\partial}{\partial r}(r^2 U j) \ , \qquad (1)$$

$$\frac{\partial \xi}{\partial t} + \frac{U}{r^2}\frac{\partial}{\partial r}(r^2\xi) = \frac{B}{4\pi\rho r^2}\frac{\partial}{\partial r}(r^2 j) \qquad (2)$$

where $j \equiv (\nabla\times\mathbf{b}_\perp)_r$ is proportional to the radial electric current density perturbation, $\xi \equiv (\nabla\times\mathbf{v}_\perp)_r$ is the radial vorticity perturbation, t is the time, and r is the heliocentric radius. The background radial magnetic field $B = B_S/\bar{r}^2$, where B_S is the magnetic field strength at the solar surface, $\bar{r} \equiv r/R_S$ is the dimensionless radial distance, and R_S is the solar radius. Because mass is conserved, the background mass density ρ and radial wind speed U are related by $\rho U r^2 = A_M$, where A_M is the constant mass flux. In principle, $U = U(r)$, which passes through the critical points, should be derived from the equations for the steady background wind [*Parker*, 1958]. For our purpose it is convenient and sufficient to prescribe $U(r)$ in the following parametric form, namely,

$$U(r) = U_* \tanh(\alpha\bar{r}^m) \qquad (3)$$

where U_* is the constant asymptotic wind speed at large radii and the two positive parameters α and m control the radial rate with which the wind speed rises from the solar surface. Note that this model is phenomenological, and it is designed just for comparison with the in situ observations of the solar wind at heliographic distances $r \gtrsim 0.3$ AU; we would emphasize that the present paper focuses on the fitting data collected at $r \gtrsim 0.3$ AU. As a consequence, the model cannot adequately describe the sub–Alfvénic region of the solar wind (where the Alfvén speed is larger than the wind speed), and indeed, we do not attempt any analysis of such a region. With this prescribed radial wind speed profile (3) the background density ρ scales as $\sim r^{-2}$ at large radii. The angular variations of j and ξ in (1) and (2) with respect to θ and ϕ are arbitrary as long as they are the same. Once j and ξ are known, one can readily obtain $\mathbf{v}_\perp(r,\theta,\phi,t)$ and $\mathbf{b}_\perp(r,\theta,\phi,t)$, respectively [*Lou*, 1993a].

Asymptotic solutions at large radii for j and ξ, and thus $\mathbf{b}_\perp$ and $\mathbf{v}_\perp$, have been previously derived by *Lou* [1993a], namely,

$$\mathbf{b}_\perp \sim r^{-3/2\pm 1/2\ (1-\omega^2/\omega_c^2)^{1/2}} \exp\left[-i\omega(r-U_* t)/U_*\right] \quad (4)$$

$$\mathbf{v}_\perp \sim r^{-1/2\pm 1/2\ (1-\omega^2/\omega_c^2)^{1/2}} \exp\left[-i\omega(r-U_* t)/U_*\right] \quad (5)$$

where the angular variations are implicit and the characteristic angular frequency ω_c is defined by [*Heinemann and Olbert*, 1980; *Barkhudarov*, 1991]

$$\omega_c = \frac{U_*}{2M_A R_S} \quad (6)$$

with $M_A \equiv B_S R_S/(4\pi A_M U_*)^{1/2}$. The WKB regime corresponds to $\omega \gg \omega_c$, while deviations from the WKB behavior appear when $\omega \lesssim \omega_c$. The main emphasis of this paper is on the non–WKB behavior of Alfvén waves as a result of background inhomogeneity in the angular frequency domain around and below $\omega = \omega_c$.

Observational studies not only focus on the quantities $\mathbf{b}_\perp$ and $\mathbf{v}_\perp$ but also on the normalized cross helicity σ_c and the Alfvén ratio $\mathcal{R}_A$ [*Matthaeus and Goldstein*, 1982a, b]. The normalized cross helicity is defined as

$$\sigma_c = \frac{-2\ \mathrm{Re} < \mathbf{b}_\perp^\dagger \cdot \mathbf{v}_\perp > /(4\pi\rho)^{1/2}}{< |\mathbf{v}_\perp|^2 > + < |\mathbf{b}_\perp|^2 > /(4\pi\rho)} \quad (7)$$

where the brackets represent average operations over relevant timescales, the dagger indicates the complex conjugate, and Re takes the real part of the complex argument. In the WKB regime, transverse velocity and magnetic field fluctuations of Alfvén waves are related by $\mathbf{v}_\perp = \mp \mathbf{b}_\perp/(4\pi\rho)^{1/2}$, where the minus and plus signs correspond to outward and inward propagations of Alfvén waves relative to the wind, respectively. The adopted sign convention in (7) is such that in the WKB regime, $\sigma_c = +1$ and $\sigma_c = -1$ correspond to outgoing and incoming Alfvén waves relative to the background radial wind, respectively. In general, $\sigma_c > 0$ and $\sigma_c < 0$ provide measures for the net outward and inward propagation of Alfvén waves, respectively.

The Alfvén ratio $\mathcal{R}_A$ is defined as the ratio of the kinetic to magnetic energy densities associated with Alfvénic fluctuations, that is,

$$\mathcal{R}_A = 4\pi\rho \frac{< |\mathbf{v}_\perp|^2 >}{< |\mathbf{b}_\perp|^2 >} \quad (8)$$

In the WKB regime, with $\omega \gg \omega_c$, $\mathcal{R}_A \to 1$ for both outward and inward propagating Alfvén waves. As we shall show presently, for angular frequency ω near ω_c and below the non–WKB behavior is pronounced. Our purpose is to compute both σ_c and $\mathcal{R}_A$ as functions of ω and r in the non–WKB regime.

3. Alfvénic Fluctuations in the Non–WKB Regime

We assume an arbitrary angular (i.e., θ and ϕ) dependence for both j and ξ and a temporal variation of the form $\exp(i\overline{\omega}\overline{t})$, where $\overline{\omega} \equiv \omega R_S/U_*$ is the dimensionless angular frequency and $\overline{t} = tU_*/R_S$ is the dimensionless time. Equations (1) and (2) for Alfvénic fluctuations can be reduced to the dimensionless form

$$\left(\frac{M_A^2}{\overline{r}^2} - \overline{U}\right)\frac{d\overline{\xi}}{d\overline{r}} = \left(i\overline{\omega} + \frac{2\overline{U}}{\overline{r}}\right)\overline{\xi} + M_A^2\left(i\overline{\omega} + \frac{d\overline{U}}{d\overline{r}}\right)\overline{j} \quad (9)$$

$$M_A^2\overline{U}\frac{d\overline{j}}{d\overline{r}} = \overline{U}\frac{d\overline{\xi}}{d\overline{r}} + \left(i\overline{\omega} + \frac{2\overline{U}}{\overline{r}}\right)\overline{\xi} - \frac{2M_A^2\overline{U}}{\overline{r}}\overline{j} \quad (10)$$

where $\overline{U} \equiv U/U_* = \tanh\ (\alpha\overline{r}^m)$, $\overline{j} = jR_S/B_S$, and $\overline{\xi} = \xi R_S/U_*$ [*Lou*, 1993a]. The above system of equations contains a singularity at the Alfvén critical point $\overline{r}_A \equiv r_A/R_S$, where the local Alfvén speed V_A and the background radial wind speed are equal. The physical solution, which passes through the Alfvén critical point $\overline{r} = \overline{r}_A$ smoothly, must satisfy the regularity condition [*Lou*, 1993a]

$$\overline{j} = -\frac{(i\overline{\omega} + 2\overline{U}/\overline{r})\overline{\xi}}{M_A^2(i\overline{\omega} + d\overline{U}/d\overline{r})} \quad (11)$$

at $\overline{r} = \overline{r}_A$. One can numerically integrate (9) and (10) starting from $\overline{r}_A$ both inwardly and outwardly to determine the global Alfvén wave solutions for various assigned values of dimensionless angular frequency $\overline{\omega}$.

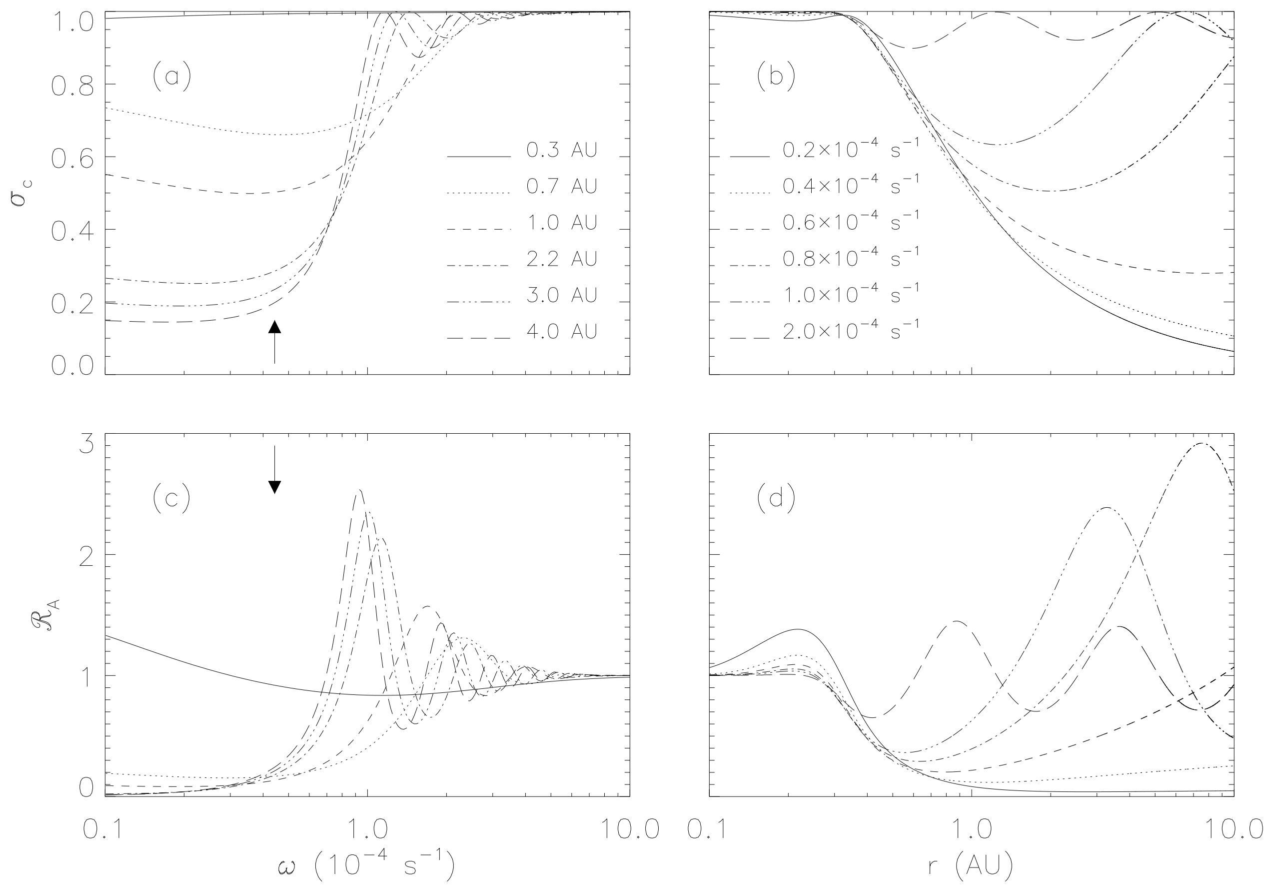

Figure 1. The normalized cross helicity σ_c (Figures 1a and 1b) and the Alfvén ratio $\mathcal{R}_A$ (Figures 1c and 1d) versus the normalized frequency for heliocentric distances r ranging from 0.3 to 4.0 AU (Figures 1a and 1c) and versus the heliocentric distance for frequencies ω ranging from 2.0×10^{-5} to 2.0×10^{-4} s^{-1} (Figures 1b and 1d). The arrows in Figures 1a and 1c point at the characteristic frequency (see text).

In order to model plausibly the polar solar wind conditions we adopt the relevant wind plasma parameters from recent Ulysses observations [*Balogh et al.*, 1995; *Phillips et al.*, 1995]. Specifically, we assumed at 1 AU that the radial wind speed $U = 7.0 \times 10^7$ cm s^{-1}, the proton number density $n_p = 3.4\,\mathrm{cm}^{-3}$, and the magnetic field strength $B = 3.5$ nT. Since the Alfvén critical radius r_A is generally inferred to fall within $\sim$ 15—50 R_S [*Pizzo et al.*, 1983; *Marsch and Richter*, 1984], the two real parameters α and m in (3) are chosen such that the Alfvén critical point r_A is located at ~ 30 R_S; thus we set $\alpha = 5.0 \times 10^{-6}$ and $m = 3.0$. The characteristic angular frequency ω_c given by (6) is estimated to be $\sim 4.4 \times 10^{-5}$ s^{-1}, which corresponds to an oscillation period of 39 hours. With this specified background wind profile we proceed to analyze the behavior of the normalized cross helicity σ_c and the Alfvén ratio $\mathcal{R}_A$ in the angular frequency range $10^{-5} \leq \omega \leq 10^{-3}$ s^{-1} and in the radial domain $0.1 \leq r \leq 10$ AU. Our results for σ_c and $\mathcal{R}_A$ associated with Alfvénic fluctuations are presented in Figure 1.

From Figure 1a, we see that $\sigma_c \leq 1.0$ for Alfvénic fluctuations in the radial solar wind. For $\omega \gtrsim 4.0 \times 10^{-4}$ s^{-1}, $\sigma_c \rightarrow 1.0$ at all radii. At the low–frequency end of the spectrum, however, σ_c can become significantly smaller than 1.0 far from the Sun. In contrast, at $r \sim 0.3$ AU, $\sigma_c \sim 1.0$ within a wide frequency range, implying the presence of purely outgoing Alfvén waves [*Roberts et al.*, 1987b; *Marsch and Tu*, 1990; *Marsch and Liu*, 1993] (Helios 1 and 2 probe solar wind properties in the inner heliosphere in the radial range $0.29 \lesssim r \lesssim 1.0$ AU. For $r \sim 0.3$ AU the magnetic field entrained in a fast wind stream around the ecliptic plane is predominantly radial, and our model analysis is valid within a large magnetic sector). At larger radii (e.g., $r \gtrsim 0.7$ AU), non–WKB behavior (i.e., continuous reflection effects) begins to manifest itself when $\omega \lesssim 3.0 \times 10^{-4}$ s^{-1}. For example, σ_c first oscillates for $10^{-4} \lesssim \omega \lesssim 3.0 \times 10^{-4}$ s^{-1} and then decreases rapidly with decreasing ω at $r \gtrsim 2$ AU. In comparison, at $r = 0.7$ AU and $r = 1.0$ AU, σ_c becomes appreciably lower than 1.0 for $\omega \lesssim 2.0 \times 10^{-4}$ s^{-1} but without apparent oscillatory behavior. The Alfvén wave oscillation period corresponding to $\omega = 2.0 \times 10^{-4}$ s^{-1} is about 10 hours.

From Figure 1c, we see the corresponding variations of the Alfvén ratio $\mathcal{R}_A$ with ω at the six different radial locations chosen for our calculations. In the high–frequency regime (i.e., $\omega \gtrsim 4.0 \times 10^{-4}$ s^{-1}), $\mathcal{R}_A \to 1$. For $7.0 \times 10^{-5} \lesssim \omega \lesssim 4.0 \times 10^{-4}$ s^{-1}, $\mathcal{R}_A$ oscillates about 1. Except for the case of $r = 0.3$ AU, $\mathcal{R}_A$ becomes much lower than 1.0 in the low–frequency end of the spectrum. We note in particular that $\mathcal{R}_A$ can be significantly larger than 1 for ω around 10^{-4} s^{-1} at radial distance $r \gtrsim 2$ AU. Note that the two arrows in both panels mark the characteristic angular frequency $\omega_c = 4.4 \times 10^{-5}$ s^{-1}.

In Figure 1b, we present radial variations of σ_c for six different values of ω. For the frequency range shown, namely, $2.0 \times 10^{-5} \leq \omega \leq 2.0 \times 10^{-4}$ s^{-1}, σ_c deviates from 1.0 for $r \gtrsim 0.4$ AU. In general, σ_c oscillates with respect to r for $\omega \gtrsim \omega_c$ and for sufficiently large r [*Lou*, 1993a]. The higher the frequency, the shorter the radial wavelength and the smaller the oscillation magnitude of σ_c. Therefore, in the high–frequency regime, $\sigma_c \to 1.0$ over the entire radial domain. For the two cases $\omega = 2.0 \times 10^{-5}$ s^{-1} (solid line) and 4.0×10^{-5} s^{-1} (dotted line), which are both less than ω_c, σ_c approaches zero with increasing radial distance r.

Figure 1d describes the radial variations of the Alfvén ratio $\mathcal{R}_A$ for the corresponding values of ω shown in Figure 1b. For an angular frequency ω around ω_c the value of $\mathcal{R}_A$ can differ from the WKB value ($\mathcal{R}_A = 1.0$) significantly. For $\omega \gtrsim \omega_c$, there is a tendency for $\mathcal{R}_A$ to oscillate with increasing r.

Our sample calculations, aimed at confronting observations of fluctuations in the high–speed polar solar wind, have revealed non–WKB behavior of σ_c and $\mathcal{R}_A$ as functions of ω and r when ω is close to ω_c. It is important to bear in mind that the fundamental cause of this non–WKB behavior for σ_c and $\mathcal{R}_A$ is continuous reflection of Alfvénic fluctuations in an inhomogeneous medium [*Heinemann and Olbert*, 1980; *Lou*, 1993a]. For the case at hand, the Alfvén speed $V_A = B/(4\pi\rho)^{1/2}$ scales as $\sim r^{-1}$ at larger radii, even though the solar wind speed is asymptotically constant. To demonstrate this point more specifically, we perform the following simple numerical experiment.

Take the case of $\omega = 10^{-4}$ s^{-1}, as shown in Figures 1b and 1d. The numerical solution of the Alfvén waves is obtained from (9) and (10) by satisfying (11) at the Alfvén critical point $\overline{r} = \overline{r}_A = 30$ for the specified background radial wind profile. Since analytic asymptotic solutions (4) and (5) for Alfvén waves at larger radii are known [*Lou*, 1993a], we match this numerical solution with a linear combination of the two asymptotic analytic solutions (i.e., the plus and minus sign solutions) at large radii in order to determine the two amplitude coefficients of the analytic solutions. We recall that the plus and minus sign solutions in both (4) and (5) correspond to net outward and inward propagation of Alfvén waves, respectively, relative to the wind when $\omega > \omega_c$. When $\omega \leq \omega_c$, the solutions with both plus and minus signs do not propagate relative to the wind, but instead, the wind advects Alfvénic fluctuations outward in the sidereal reference frame. We also recall that at the Alfvén critical point r_A the regularity condition (11) implies net locally outgoing waves. Precisely because the background wind is radially inhomogeneous, net inward propagating waves relative to the wind are continuously generated at large radii [*Heinemann and Olbert*, 1980]; the relative importance of inward propagating Alfvén waves as compared to outward propagating Alfvén waves is frequency dependent. Once the two amplitude coefficients are determined, one can compute σ_c and $\mathcal{R}_A$ directly from the linear combination of the two asymptotic analytic solutions (4) and (5). A comparison of σ_c and $\mathcal{R}_A$ (dashed lines) thus computed with σ_c and $\mathcal{R}_A$ (solid lines) obtained from the numerical solution is shown in Figure 2. The agreement between the analytical and numerical solutions becomes very good for $r \gtrsim 0.3$ AU; the significant deviations at small radii (i.e., $r \lesssim 0.3$ AU) are not surprising because the analytic solutions (4) and (5) are expected to be valid only at sufficiently large values of r so that the radial wind speed $U(r)$ becomes nearly constant. The oscillatory behavior of both σ_c and $\mathcal{R}_A$ is caused by the interference of net inward and outward propagating Alfvén waves relative to the wind. This essential point can be readily understood with the help of the analytic expression for the normalized cross helicity at sufficiently large r [*Lou*, 1993a]

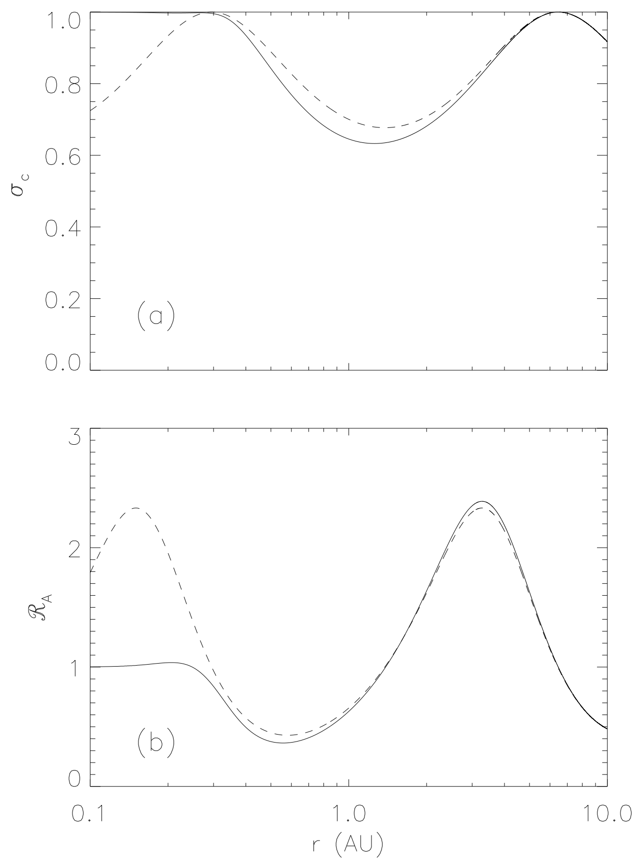

Figure 2. (a) The normalized cross helicity σ_c and (b) the Alfvén ratio $\mathcal{R}_A$ versus the heliocentric distance for a single–frequency Alfvén wave with $\omega = 10^{-4}\ \mathrm{s}^{-1}$. The numerical solution (solid lines) and the asymptotic analytical solution at a large radial distance (dashed lines) are presented.

$$\sigma_c \sim -(1-f_c^2/f^2)^{1/2}(\bar\omega^2|b_0|^2-|a_0|^2)\left\{|a_0|^2+\bar\omega^2|b_0|^2 -\bar\omega\mathrm{Re}\left[\left(ia_0^\dagger b_0/(\lambda_+ +1)\right)\bar r^{i(f^2/f_c^2-1)^{1/2}}\right]\right\}^{-1} \quad (12)$$

with $\lambda_\pm = -3/2 \pm (1/2)[1-(f/f_c)^2]^{1/2}$. According to equations (111) and (112) of *Lou* [1993a], similar oscillatory terms, such as $\cos[(f^2/f_c^2-1)^{1/2}\ln r]$ or $\sin[(f^2/f_c^2-1)^{1/2}\ln r]$, are present in the Alfvén ratio $\mathcal{R}_A$:

$$\mathcal{R}_A = \frac{u_\infty M_{AS}}{V_{AS}\bar\omega^2}\Big[|a_0|^2\bar r^{2(\mathrm{Re}\{\lambda_-\}+1)} +\bar\omega^2|b_0|^2\bar r^{2(\mathrm{Re}\{\lambda_+\}+1)} + 2\mathrm{Re}\left(ia_0^\dagger b_0\bar\omega\bar r^{(\lambda_-^\dagger+\lambda_++2)}\right)\Big] \cdot\left[\frac{|a_0|^2\bar r^{2(\mathrm{Re}\{\lambda_-\}+1)}}{|\lambda_-+1|^2}+\frac{\bar\omega^2|b_0|^2\bar r^{2(\mathrm{Re}\{\lambda_+\}+1)}}{|\lambda_++1|^2} +2\mathrm{Re}\left(\frac{ia_0^\dagger b_0\bar\omega\bar r^{(\lambda_-^\dagger+\lambda_++2)}}{(\lambda_-^\dagger+1)(\lambda_++1)}\right)\right]^{-1} \quad (13)$$

By the example of Figure 2, we conclude that the oscillatory behavior of σ_c and $\mathcal{R}_A$ shown in Figure 1 originate from continuous reflection of Alfvén waves in the inhomogeneous background radial wind.

4. Comparison with Helios Observations

The model calculations discussed in section 3 can be readily compared with observations, especially near the solar poles (where our model assumptions and approximations are best satisfied). Although the equatorial solar wind within $\pm 30°$ is somewhat complex in contrast to the remarkably steady polar solar wind, it is nevertheless tempting to compare results of our model calculations with earlier analyses of fluctuation data from the Helios 1 (December 1974 to February 1986) and Helios 2 (January 1976 to March 1980) spacecrafts, which covered the radial range between 0.29 and 1.0 AU. Our main purpose here is to examine whether the relatively strong reflection effects of Alfvén waves around the characteristic angular frequency ω_c defined by (6) are already discernible in the Helios 1 and 2 data. In general, one would expect that our model is more appropriate for Alfvénic fluctuations in fast streams within large magnetic sectors close to the Sun and that deviations from our model calculations should systematically appear with increasing radial distance as a result of the gradual formation of a spiral magnetic field, as well as other complications. With these caveats in mind we proceed to the comparison study.

4.1. Fluctuations in the Fast–Stream Solar Wind

We consider Helios observations of fluctuations in fast streams as described by *Bruno at al.* [1985] and *Marsch and Tu* [1990]. Measured wind parameters by both Helios 1 and 2 are taken from Table 1a of *Marsch and Tu* [1990] and Table 1 of *Bruno et al.* [1985] and are summarized in our Tables 1 and 2, respectively. Although the solar wind parameters in Tables 1 and 2 are given at different times and radii, one must nevertheless determine a sensible reference background wind on the basis of these parameters in order to proceed. We thus use the equations for conservation of mass ($\rho U r^2 = A_M \equiv$ constant mass flux) and magnetic flux ($Br^2 = F_B \equiv$ constant magnetic flux), assuming a constant radial wind speed profile $U(r)$ far from the Sun ($r \gtrsim 0.3$ AU), to fit the Helios data contained in Tables 1 and 2. This fit allows us to determine the values of velocity U_*, proton number density n_{p*}, and magnetic field B_* at 1 AU. Then, we use the parametric form (3) for the radial wind speed profile $U(r)$ to fit the Helios data contained in Tables 1 and 2 and to reproduce the observed behavior of the normalized cross helicity σ_c and Alfvén ratio $\mathcal{R}_A$. After some trials and adjustments the reference wind profile, together with the available Helios data points, are shown in Figure 3. This "best fit" reference model appears to give a rather reasonable description of the mean Helios data. The relevant fitting parameters in formula (3) and the physical parameters which characterize the wind model are summarized in Table 3. This table also contains the parameters characterizing the wind model which fits the slow–stream solar wind discussed in the next section.

Table 1. Relevant Parameters for Fast Streams Taken From Table 1a of *Marsch and Tu* [1990] for Helios 2 in 1976

r, AU	U, km s^{-1}	n_p, cm^{-3}	B, nT	V_A, km s^{-1}
0.29	708	30.0	–	136
0.65	621	6.0	–	79
0.87	632	4.0	–	59

The r is the heliocentric distance; U is the measured wind speed; n_p is the proton number density; B is the magnetic field strength; and V_A is the local Alfvén speed.

Given this fast stream reference radial wind profile, we can readily obtain numerical solutions over a wide frequency range (i.e., 10^{-6} s^{-1} $\leq f \leq 10^{-2}$ s^{-1}) for Alfvén waves between 0.1 and 1.0 AU by using (9) and (10) with the regularity condition (11) imposed at the Alfvén critical point $\bar{r}_A \equiv r_A/R_S = 16$. In Figure 4 the normalized cross helicity σ_c as defined by (7) and the Alfvén ratio $\mathcal{R}_A$ as defined by (8) are presented as functions of frequency f at three different radial locations, namely, 0.29 (solid line), 0.65 (dotted line), and 0.87 AU (dashed line). The arrows in Figures 4a and 4b indicate the locations of the characteristic frequency $f_c = 6.2 \times 10^{-6}$ s^{-1}. It is possible to compare our Figure 4a with the right three panels (i.e., fast streams) of Figure 4 of *Marsch and Tu* [1990] and our Figure 4b with the right three panels (i.e., fast streams) of Figure 7 of *Marsch and Tu* [1990]; furthermore, it is possible to compare our Figure 4b with Figure 5 of *Bruno et al.* [1985], where the inverse of the Alfvén ratio $\mathcal{R}_A^{-1}$ is reported.

Table 2. Relevant Parameters Taken From Table 1 of *Bruno, et al.* [1985] for Helios 1 in 1975 and Helios 2 in 1976

r, AU	U, km s^{-1}	n_p, cm^{-3}	B, nT	V_A, km s^{-1}
		Helios 1		
0.31	623	33.95	34.02	127
0.62	672	7.39	8.56	69
0.87	710	3.24	4.54	55
		Helios 2		
0.29	727	28.88	33.12	134
0.65	633	6.43	8.58	74
0.88	630	3.85	5.39	60

Notations are as in Table 1.

Table 3. Parameters for the Wind Models Fitting the Fast– and Slow–Stream Solar Wind

	Fast Stream	Slow Stream
U_*, km s^{-1}	660	431
n_{p*}, cm^{-3}	2.74	8.0
B_*, nT	3.16	4.7
α	10^{-5}	10^{-5}
m	4	2.7
M_A^2	147	262
r_A, in units of r_S	16	38
f_c, 10^{-6} s^{-1}	6.2	3.0

Discussed in subsections 4.1 and 4.2.

Variables are as follows: U_*, radial speed wind; n_{p*}, proton number density; B_*, radial magnetic field strength at 1 AU; α and m, the parameters in formula (3); $M_A \equiv B_S R_S/(4\pi A_M U_*)^{1/2}$; r_A, the Alfvén critical radius; and $f_c \equiv \omega_c/(2\pi)$, the characteristic frequency.

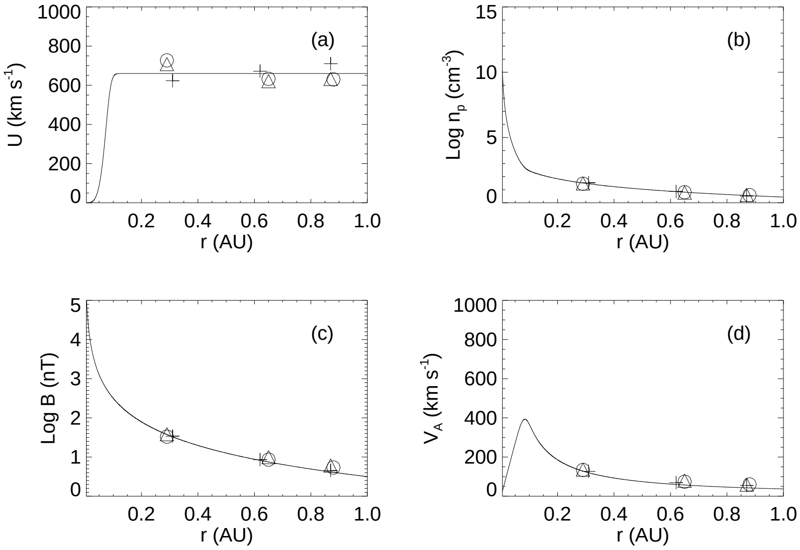

Figure 3. The reference wind profile for fast–stream solar wind as fitted with available data points from spacecraft Helios 1 and 2. The radial wind speed $U(r)$, the radial magnetic field B, the proton number density n_p, and the radial Alfvén wave speed V_A as functions of heliocentric radius up to 1 AU are shown in Figures 3a, 3b, 3c, and 3d, respectively. The crosses and the circles are the data taken from Helios 1 and 2, respectively [*Bruno et al.*, 1985], and the triangles are the data taken from Helios 2 [*Marsch and Tu*, 1990].

By examining the right three panels for the measured σ_c in Figure 4 of *Marsch and Tu* [1990] and for the computed σ_c of our Figure 4a, we note that the behavior of σ_c appears qualitatively similar at the low–frequency end, around the characteristic frequency f_c, although for the case of $r = 0.87$ AU, the computed σ_c does not drop drastically to a negative value around $f \sim 6.0\times10^{-6}$ s^{-1} as shown in the data. For example, in the low–frequency end of the spectrum the computed σ_c increases with increasing f and reaches $\sim$1.0 around $f \sim 3.0 \times 10^{-5}$ s^{-1} at $r = 0.29$ AU. Furthermore, a weak oscillatory behavior of σ_c is present in the data around $f \sim 2.0\times10^{-5}$ s^{-1}. On the basis of this comparison we conclude that there is some evidence in the Helios data for the enhanced reflection of Alfvén waves in fast wind streams around the characteristic frequency f_c. The data also show a subtle feature in that the nearly constant σ_c within the frequency range 10^{-4} s$^{-1} \lesssim f \lesssim 10^{-3}$ s^{-1} tends to decrease slightly with increasing r; our computed σ_c with a value very close to 1.0 does not show this effect within the same frequency range. The high–frequency falloff of σ_c (i.e., $f \gtrsim 10^{-3}$ s^{-1}) shown in the data might be caused by effects such as dissipation, nonlinear cascades, and conversion from magnetic to kinetic energies. Since (9) and (10) for Alfvén waves are dissipationless and linear, the computed σ_c remains close to unity when f is sufficiently larger than f_c: in other words, these equations cannot, in principle, account for such effects.

The computed Alfvén ratios $\mathcal{R}_A$ presented in Figure 4b show pronounced oscillatory behavior within the frequency range $\sim 10^{-5}$ s$^{-1} \lesssim f \lesssim 10^{-4}$ s^{-1}; the oscillation amplitudes of $\mathcal{R}_A$ become larger as f is lowered toward f_c. In comparison, the data for $\mathcal{R}_A$ contained in the right three panels of Figure 7 of *Marsch and Tu* [1990] reveal a similar tendency of increasing $\mathcal{R}_A$ in the low–frequency end of the fluctuation spectrum; except for the case of $r = 0.29$ AU the oscillatory signature in $\mathcal{R}_A$ is, however, fairly weak. Within the frequency range $\sim 5.0 \times 10^{-5}$ s$^{-1} \lesssim f \lesssim 2.0 \times 10^{-3}$ s^{-1} the observed $\mathcal{R}_A$ is fairly constant at a given radial location but tends to decrease with increasing r; that is, $\mathcal{R}_A \sim 1.0$ at $r = 0.29$ AU, and $\mathcal{R}_A \sim 0.7$ at $r = 0.65$ AU, $\mathcal{R}_A \sim 0.5$ at $r = 0.87$ AU. In contrast, our computed $\mathcal{R}_A$ remains very close to ~ 1.0 for $f \gtrsim 10^{-4}$ s^{-1} at all radial locations. Although somewhat crude, we regard the low–frequency increase of $\mathcal{R}_A$ shown in the data as consistent with relatively strong reflections of Alfvén waves in fast wind streams.

An analogous result is in Figure 5 of *Bruno et al.* [1985], where the inverse of the Alfvén ratio $\mathcal{R}_A^{-1}$ is reported. Although the data from Helios 1 and 2 do not show the significant increase of $\mathcal{R}_A^{-1}$ very close the characteristic frequency f_c, as displayed in our Figure 4b, weak oscillations in $\mathcal{R}_A^{-1}$ around the low–frequency end of the spectrum seem to exist in the data. In the domain of sufficiently high frequencies the observed $\mathcal{R}_A^{-1}$ tends to increase with increasing r, which is consistent with the data analysis of *Marsch and Tu* [1990].

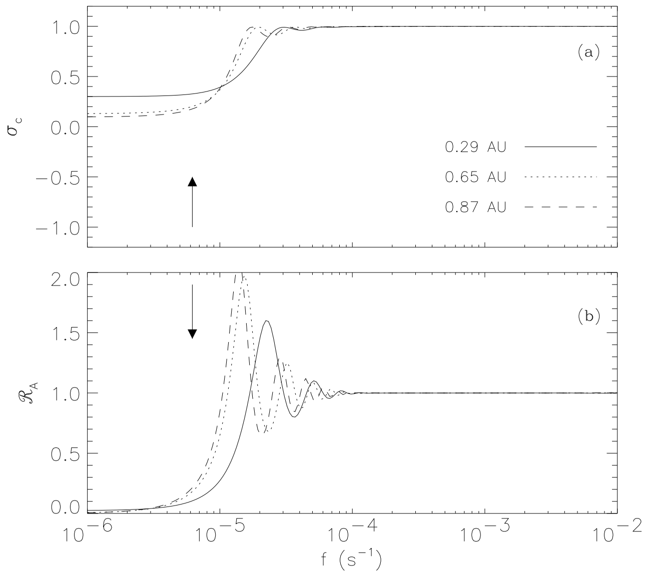

Figure 4. For the parameters of the fitted reference fast–wind profile shown in Figure 3 we present (a) the normalized cross helicity σ_c defined by (7) and (b) the Alfvén ratio $\mathcal{R}_A$ defined by (8) computed at three different radial locations and in a wide frequency range including the characteristic frequency $f_c = 6.2 \times 10^{-6}$ s^{-1} (marked by the arrows). The solid, dotted, and dashed lines correspond to the numerical results at radial locations of 0.29, 0.65, and 0.87 AU, respectively.

To briefly summarize, we note that in all these comparisons of our model results for σ_c and $\mathcal{R}_A$ around the characteristic frequency $f_c = 6.2 \times 10^{-6}$ s^{-1} with fluctuation data in the fast–stream solar wind from Helios 1 and 2 the best fit comes with $r \sim 0.3$ AU. This is not surprising because our background radial wind model works better at smaller radii than at larger radii.

4.2. Fluctuations in the Slow–Stream Solar Wind

We now turn to a comparison of observed fluctuations in the slow–stream solar wind by spacecraft Helios 1 and 2 [*Roberts et al.*, 1987b; *Marsch and Tu*, 1990] with our model calculations. The available data points for constructing the reference slow radial wind profile is summarized in Table 4.

We proceed as in subsection 4.1 to determine the wind profile which fits the Helios data contained in Table 4. The reference slow radial wind profile thus obtained is shown in Figure 5, and the parameters characterizing the model are summarized in Table 3. Again, the best fit reference model gives a fairly good account of the slow wind mean properties.

Table 4. Relevant Parameters for Slow Winds Taken From Table 1a of *Marsch and Tu* [1990] for Helios 2 in 1976

r, AU	U, km s^{-1}	n_p, cm^{-3}	B, nT	V_A, km s^{-1}
0.31	422	123.0	–	61
0.69	420	13.0	–	65
0.89	452	10.0	–	46

Notations are as in Table 1.

Numerical solutions for Alfvén waves in such a slow reference wind are obtained from (9) and (10) with the regularity condition (11) imposed at the Alfvén critical point at $\bar{r}_A = 48$. On the basis of these solutions we compute σ_c and $\mathcal{R}_A$ within the frequency range 10^{-6} s$^{-1} \lesssim f \lesssim 10^{-2}$ s^{-1} at three different radial locations r = 0.31, 0.69, and 0.89 AU. These results are shown in Figure 6 in which arrows mark the characteristic frequency $f_c = 2.6 \times 10^{-6}$ s^{-1}.

A comparison of the computed σ_c in our Figure 6a with the left three panels in Figure 4 of *Marsch and Tu* [1990] reveals apparent differences. Even in the high–frequency domain, the observed σ_c is significantly lower than 1.0. Except for the case of r = 0.69 AU the observed σ_c becomes negative around the low–frequency end of the spectrum. The disagreement between the computed $\mathcal{R}_A$ in our Figure 6b and the left three panels in Figure 7 of *Marsch and Tu* [1990] is also not easy to reconcile. Within the frequency range $10^{-4} \lesssim f \lesssim 3.0 \times 10^{-3}$ s^{-1} the observed $\mathcal{R}_A$ is significantly less than 1.0 (i.e., at the three different radial locations, $\mathcal{R}_A \sim 0.5$), although there exists a clear tendency in the data for a significant increase of $\mathcal{R}_A$ slightly above $f \sim 10^{-5}$ s^{-1}.

Roberts et al. [1987a, b] performed extensive solar wind fluctuation data analyses and comparisons on the basis of observations from Voyager and Helios spacecraft. The data presentations in Figures 1 and 2 of *Roberts et al.* [1987b] offer a useful complementary

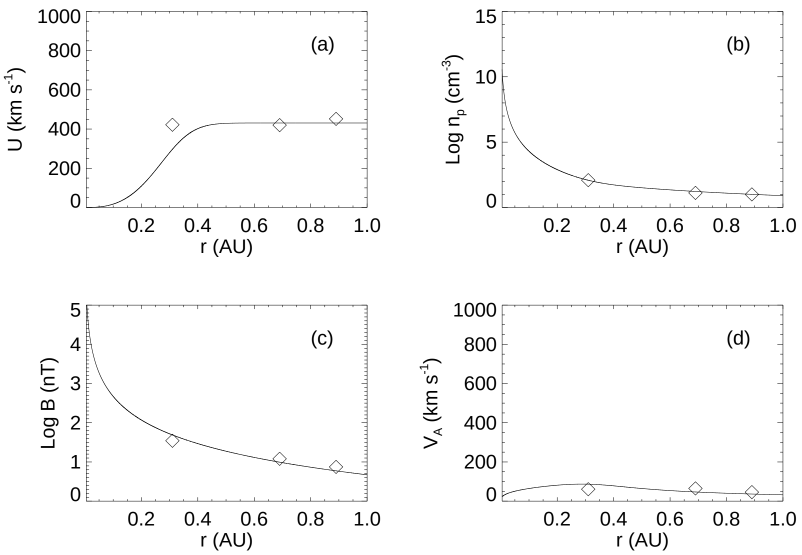

Figure 5. As in Figure 3 for the reference wind profile for slow–stream solar wind as fitted with available data points from spacecraft Helios 2 [*Marsch and Tu*, 1990]. The diamonds are the data points from Helios 2 in 1976.

perspective to what is displayed in Figure 4 of *Marsch and Tu* [1990], although the spectral information in the results of *Roberts et al.* [1987b] is somewhat coarse [*Roberts et al.*, 1987a; *Owens*, 1977]. In particular, we emphasize that the frequency variations of the normalized cross helicity σ_c can be qualitatively different at two relatively nearby radii (or two different epochs); for example, slightly to the left and right of day 80 (i.e., $r \sim 0.65$ AU) in Figure 1 of *Roberts et al.* [1987b] for Helios 1 data in early 1980, the variations of σ_c with frequency are quite different. In other words, there apparently exist "good" and "bad" time intervals for signals of Alfvénic fluctuations. We therefore caution that the left three panels in Figure 4 of *Marsch and Tu* [1990] for σ_c determined from Helios 2 data in slow solar wind might be subject to a similar selection effect.

While we have not attempted to construct a reference slow–wind profile from the Helios 1 and 2 data of *Roberts et al.* [1987b], we shall nevertheless qualitatively compare our computed results of σ_c in Figure 6 with the data shown in their Figures 1 and 2. Around $r \sim 0.3$ AU, the frequency variation of σ_c shown in their Figure 1 is similar to the solid line (i.e., the case of $r = 0.31$ AU) in our Figure 6a, although the low–frequency falloff of our computed σ_c is not as that significant as shown in their data. Around $r \sim 0.7$ AU, the frequency variation of σ_c shown in their Figure 1 is similar to the dotted line (i.e., the case of $r = 0.69$ AU) in our Figure 6a, except for the lowest frequency point at $f \sim 1.1 \times 10^{-6}$ s^{-1} where their data show $\sigma_c \sim 0$. Similarly, around $r \sim 0.9$ AU, the frequency variation of σ_c shown in their Figure 1 is similar to the dashed line (i.e., the case of $r = 0.89$ AU) in our Figure 6a, except for the lowest frequency point at $f \sim 1.1 \times 10^{-6}$ s^{-1} where their data again show $\sigma_c \sim 0$. One can also carry out similar comparisons of our computed σ_c in panel (a) of Figure 6 with Figure 5a for Helios 2 near 0.7 AU and Figure 7a for Helios 1 near 0.6 AU of *Roberts et al.* [1987b]. Finally, we note that when one examines Figure 2 of *Roberts et al.* [1987b], one finds that during periods of significant Alfvénic fluctuations (namely, near day 10 or near $r \sim 0.33$ AU), there is an extended period during which the frequency variation of σ_c is similar to the solid line in our Figure 6a, although the low–frequency falloff of our computed σ_c is not as significant as that shown in the data. Likewise, around $r \sim 0.67$ AU (that is, around day 40), the frequency variation of σ_c is similar to the dotted line in our Figure 6a, although $\sigma_c \sim 0.3$ at $f \sim 1.1 \times 10^{-6}$ s^{-1} shown in their data is much lower than our computed σ_c around that frequency.

In Figure 7 we present radial variations of σ_c, and $\sigma_z \equiv (\mathcal{R}_A - 1)/(\mathcal{R}_A + 1)$ for the slow wind profile (see Figure 5) at four different frequencies, namely, 9.3×10^{-5} (solid line), 1.0×10^{-5} (dotted line), 3.4×10^{-6} (dashed line), and 1.1×10^{-6} s^{-1} (dash–dotted line), corresponding to periods of 3, 27, 81, and 243 hours, respectively. The solid line in Figure 7a fits well to the overall envelopes of $\sigma_c(3)$ at the 3–hour timescale (*Roberts et al.* [1987b] noted that the 9–hour timescale $\sigma_c(9)$ looks qualitatively the same as the 3–hour timescale $\sigma_c(3)$) in both Figures 1 and 2 of *Roberts et al.* [1987b]; the dotted line 7a agrees with the overall envelopes of $\sigma_c(27)$ at the 27–hour timescale in both Figures 1 and 2 of *Roberts et al.* [1987b], although $\sigma_c(27)$ does appear somewhat lower than our computed σ_c around 1 AU. Finally, the dashed line in 7a shows a similar falloff with radial distance as the overall envelopes of $\sigma_c(81)$ at the 81–hour timescale in both Figures 1 and 2 of *Roberts et al.* [1987b], but $\sigma_c(81)$ does appear to be systematically lower than our computed σ_c. At the 243–hour timescale, there is no agreement between our results and the analysis of *Roberts et al.* [1987b].

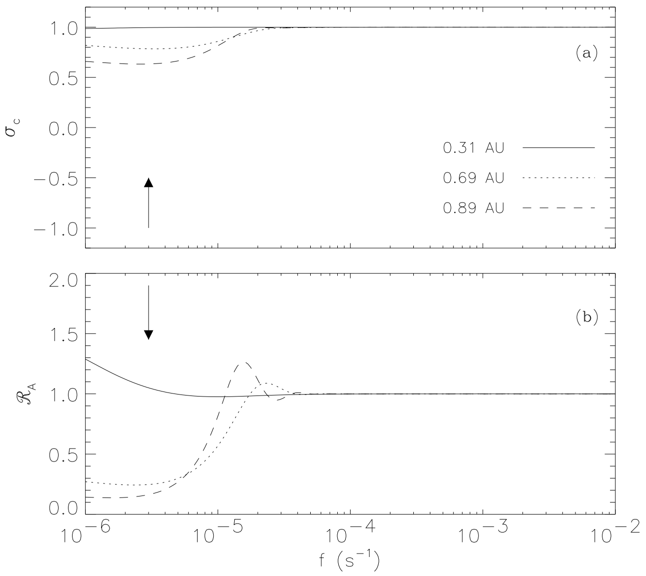

Figure 6. As in Figure 4 for the parameters of the fitted reference slow–wind profile shown in Figure 5.

The quantity $\sigma_z \equiv (\mathcal{R}_A - 1)/(\mathcal{R}_A + 1)$ is shown in Figure 3 of *Roberts et al.* [1987b] only on two different timescales, namely, 3 and 248 hours. The comparison of computed σ_z in our Figure 7b with their Figure 3 reveals a complete mismatch. While the disagreement for σ_z on the 248–hour timescale is not surprising, the disagreement for σ_z on the 3–hour timescale is unexpected because the agreement for σ_c on the 3–hour timescale is generally good over many time intervals. From the theoretical viewpoint for Alfvénic fluctuations, $\sigma_c \sim 1$ would imply $\mathcal{R}_A \sim 1$ and thus $\sigma_z \sim 0$. The 3–hour timescale data of *Roberts et al.* [1987b] show instead that for σ_c of the order of 1.0, $\mathcal{R}_A$ can be much less than 1.0 such that σ_z is close to ~ -1.0. We do not understand as yet the origin of this discrepancy but suspect that the presence of significant Alfvénic turbulence could be responsible.

To conclude, we note that our theoretical results for σ_c fit the data well during periods of strong Alfvénic fluctuations. Under these conditions the agreement tends to be better for shorter timescales and closer distances to the Sun, which we would expect in the context of our model. At the longest timescale (that is, 243 hours) the disagreement between our theory and Helios data is strong; to what extent this problem is due to inadequate sampling in the space–time domain by the spacecraft (which moves $\sim$0.1 AU on this timescale) is as yet unclear.

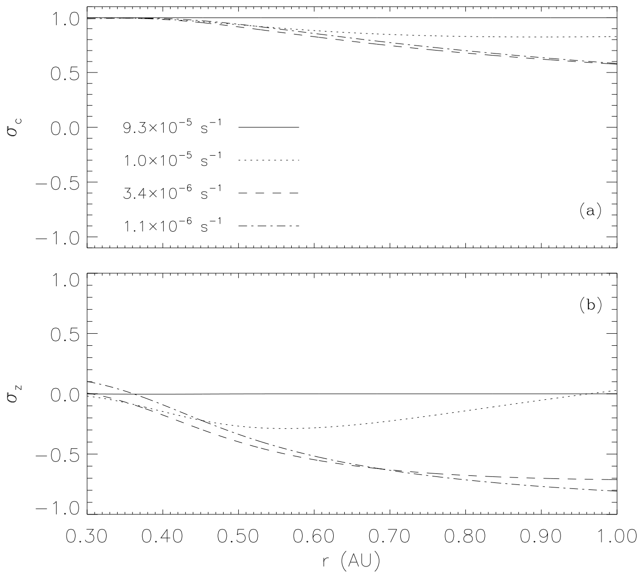

Figure 7. For the parameters of the fitted reference slow–wind profile shown in Figure 5 we present (a) the normalized cross helicity σ_c defined by (7) and (b) the σ_z related to the Alfvén ratio (lower panel) computed for different frequencies and in the radial range $0.3\ \mathrm{AU} \lesssim r \lesssim 1.0\ \mathrm{AU}$. The solid, dotted, dashed, and dash–dotted lines in each panel correspond to the numerical results at frequencies of 9.3×10^{-5}, 1.0×10^{-5}, 3.4×10^{-6}, and $1.1 \times 10^{-6}\ \mathrm{s}^{-1}$, respectively.

5. Summary

We have computed the normalized cross helicity σ_c, the Alfvén ratio $\mathcal{R}_A$, and other related quantities associated with Alfvénic fluctuations in a background radial wind with spherical symmetry and radial magnetic field. In particular, we have presented the frequency and radial variations of σ_c and $\mathcal{R}_A$ as well as of other related quantities in the frequency range near the characteristic angular frequency ω_c. As a result of continuous reflections of Alfvén waves in the inhomogeneous background radial wind [e.g., *Heinemann and Olbert*, 1980], σ_c and $\mathcal{R}_A$ exhibit pronounced non–WKB behavior in this frequency regime.

We wish to emphasize that the wind model we used is a phenomenological one designed just for comparison with the Ulysses and Helios observations; as such, it depends only on a few, easy to handle, parameters in order to provide simple straightforward information amenable to being used, at a later time, with more complex and harder to handle models. As a consequence, the model cannot adequately describe the sub–Alfvénic portion of the solar wind, and indeed, we did not attempt any analysis of such a region. On the other hand, we were concerned with fitting data collected at $\gtrsim 0.29$ AU, that is, in the super–Alfvénic portion of the wind.

We compare our theoretical results with earlier data analyses of observations from the Helios 1 and 2 spacecraft [*Bruno et al.*, 1985; *Roberts et al.*, 1987b; *Marsch and Tu*, 1990] and find evidence for continuous reflections of Alfvén waves around the characteristic frequency ω_c in the fast–speed solar wind close to the Sun but only very weak evidence of this sort in the slow–speed solar wind. Our analysis indicates that long–period Alfvénic fluctuations could persist around ~ 0.3 AU which is consistent with observations [*Denskat and Neubauer*, 1982; *Bruno et al.*, 1985; *Roberts et al.*, 1987b; *Marsch and Tu*, 1990; *Marsch and Liu*, 1993]. We anticipate that comparisons with Ulysses data [e.g., *Balogh et al.*, 1995; *Smith et al.*, 1995b] for flows from the solar poles might be of considerable interest because our model is a much more appropriate description for these cases.

Acknowledgments. S. Orlando acknowledges the hospitality of the Dept. of Astronomy and Astrophysics, The University of Chicago, where a crucial part of the present work was carried out. This work was supported in part by Ministero della Università e della Ricerca Scientifica e Tecnologica, GNA–CNR, and Regione Siciliana, and in part by NSF and NASA grants to the University of Chicago.

The editor thanks A. Barnes and D. B. Melrose for their assistance in evaluating this paper.

References

Balogh A., E. J. Smith, B. T. Tsurutani, D. J. Southwood, R. J. Forsyth, and T. S. Horbury, The heliospheric magnetic field over the south polar region of the Sun, *Science, 268*, 1007, 1995.

Barkhudarov, M. R., Alfvén waves in stellar winds, *Solar Phys., 135*, 131, 1991.

Barnes, A., Hydromagnetic waves and turbulence in the solar wind, in *Solar System Plasma Physics*, vol. 1, edited by C. F. Kennel, L. J. Lanzerotti, and E. N. Parker, pp. 249–319, North–Holland, New York, 1979.

Bavassano, B., and E. J. Smith, Radial variations of interplanetary Alfvénic fluctuations: Pioneer 10 and 11 observations between 1 and 5 AU, *J. Geophys. Res., 91*, 1706, 1986.

Belcher, J. W., L. Davis Jr., and E. J. Smith, Large–amplitude Alfvén waves in the interplanetary medium: Mariner 5, *J. Geophys. Res., 74*, 2302, 1969.

Belcher, J. W., and L. Davis Jr., Large–amplitude Alfvén waves in the interplanetary medium, 2, *J. Geophys. Res., 76*, 3534, 1971.

Bruno, R., B. Bavassano, and U. Villante, Evidence for long–period Alfvén waves in the inner solar system, *J. Geophys. Res., 90*, 4373, 1985.

Coleman, P. J., Jr., Turbulence, viscosity and dissipation in the solar wind plasma, *Astrophys. J., 153*, 371, 1968.

Denskat, K. U., and F. M. Neubauer, Statistical properties of low–frequency magnetic field fluctuations in the solar wind from 0.29 to 1.0 AU during solar minimum conditions: Helios 1 and Helios 2, *J. Geophys. Res., 87*, 2215, 1982.

Geiss, J., et al., The southern high–speed stream: Results from the SWICS instrument on Ulysses, *Science, 268*, 1033, 1995.

Goldstein, M. L., D. A. Roberts, and W. H. Matthaeus, Magnetohydrodynamic turbulence in the solar wind, *Ann. Rev. Astron. Astrophys., 33*, 283, 1995.

Grall, R. R., W. A. Coles, M. T. Klinglesmith, A. R. Breen, P. J. S. Williams, J. Markkanen, and R. Esser, Rapid acceleration of the polar solar wind, *Nature, 379*, 429, 1996.

Heinemann, M., and S. Olbert, Non–WKB Alfvén waves in the solar wind, *J. Geophys. Res., 85*, 1311, 1980.

Hollweg, J. V., Some physical processes in the solar wind, *Rev. Geophys., 16*, 689, 1978.

Holzer, T. E., Effects of rapidly diverging flow, heat addition, and momentum addition in the solar wind and stellar winds, *J. Geophys. Res., 82*, 23, 1977.

Jokipii, J. R., and J. Kóta, The polar heliospheric magnetic field, *Geophys. Res. Lett., 16*, 1, 1989.

Keppler, E., M. Fränz, A. Korth, M. K. Reuss, J. B. Blake, R. Seidel, J. J. Quenby, and M. Witte, Observations of energetic particles with EPAC on Ulysses in polar latitudes of the heliosphere, *Science, 268*, 1013, 1995.

Lanzerotti, L. J., et al., Over the southern solar pole: Low–energy interplanetary charged particles, *Science, 268*, 1010, 1995.

Lou, Y. Q., Three–dimensional magnetic field configurations in the heliosphere, *J. Geophys. Res., 97*, 17,183, 1992a.

Lou, Y. Q., Three–dimensional Alfvénic perturbations in the solar wind, in *Proceedings of the 1992 Cambridge Workshop in Theoretical Geoplasma Physics*, edited by

T. Chang and J. R. Jasperse, Scientific Publischers, Inc., Cambridge, MA, p. 453, 1992b.

Lou, Y. Q., Propagation of three–dimensional Alfvén waves and its nonlinear effects in the solar wind, *J. Geophys. Res., 98*, 3563, 1993a.

Lou, Y. Q., Three–dimensional nonsteady compressible magnetohydrodynamic fluctuations in the solar wind, *J. Geophys. Res., 98*, 11,483, 1993b.

Lou, Y. Q., Alfvénic disturbances in the equatorial solar wind with a spiral magnetic field, *J. Geophys. Res., 99*, 14,747, 1994.

Lou, Y. Q., On two–component models of solar wind fluctuations, *J. Geophys. Res., 100*, 5877, 1995.

Lou, Y. Q., Corotating shock accelerated particles guided by wavy spiral magnetic fields in the solar wind at high heliographic latitudes, *Geophys. Res. Lett., 23*, 609, 1996.

Marsch, E., and S. Liu, Structure functions and intermittency of velocity fluctuations in the inner solar wind, *Ann. Geophys., 11*, 227, 1993.

Marsch, E., and A. K. Richter, Distribution of solar wind angular momentum between particles and magnetic field: Inferences about the Alfvén critical point from Helios observations, *J. Geophys. Res., 89*, 5386, 1984.

Marsch, E., and C.–Y. Tu, On the radial evolution of MHD turbulence in the inner heliosphere, *J. Geophys. Res., 95*, 8211, 1990.

Marsch, E., and C.–Y. Tu, Modeling results on spatial transport and spectral transfer of solar wind alfvénic turbulence, *J. Geophys. Res., 98*, 21,045, 1993.

Matthaeus, W. H., and M. L. Goldstein, Measurement of the rugged invariants of magnetohydrodynamic turbulence in the solar wind, *J. Geophys. Res., 87*, 6011, 1982a.

Matthaeus, W. H., and M. L. Goldstein, Stationarity of magnetohydrodynamic fluctuations in the solar wind, *J. Geophys. Res., 87*, 10,347, 1982b.

Matthaeus, W. H., M. L. Goldstein, and D. A. Roberts, Evidence for the presence of quasi–two–dimensional nearly incompressible fluctuations in the solar wind, *J. Geophys. Res., 95*, 20,673, 1990.

Munro, R. H., and B. V. Jackson, Geometry and density of a polar coronal hole, *Astrophys. J., 213*, 874, 1977.

Orlando, S., Y. Q. Lou, R. Rosner, and G. Peres, Propagation of three–dimensional Alfvén waves in a stratified, thermally conducting solar wind, *J. Geophys. Res., 101*, 24,443, 1996.

Owens, A. J., The nested variance power spectrum, *J. Geophys. Res., 82*, 3315–3318, 1977.

Parker, E. N., Dynamics of the interplanetary gas and magnetic fields, *Astrophys. J., 128*, 664, 1958.

Phillips J. L., S. J. Bame, W. C. Feldman, B. E. Goldstein, J. T. Gosling, C. M. Hammond, D. J. McComas, M. Neugebauer, E. E. Scime, and S. T. Suess, Ulysses solar wind plasma observations at high southerly latitudes, *Science, 268*, 1030, 1995.

Pizzo, V., R. Schwenn, E. Marsch, H. Rosenbauer, K.–H. Mühlhäuser, and F. M. Neubauer, Determination of the solar wind angular momentum flux from the Helios data – An observational test of the Weber and Davis theory, *Astrophys. J., 271*, 335, 1983.

Roberts, D. A., and M. L. Goldstein, Turbulence and waves in the solar wind, *U.S. Natl. Rep. Int. Union Geod. Geophys. 1987–1990*, *Rev. Geophys., 29*, 932, 1991.

Roberts, D. A., L. W. Klein, M. L. Goldstein, and W. H. Matthaeus, The nature and evolution of magnetohydrodynamic fluctuations in the solar wind: Voyager observations, *J. Geophys. Res., 92*, 11,021, 1987a.

Roberts, D. A., M. L. Goldstein, L. W. Klein, and W. H. Matthaeus, Origin and evolution of fluctuations in the solar wind: Helios observations and Helios–Voyager comparisons, *J. Geophys. Res., 92*, 12,023, 1987b.

Simpson, J. A., et al., Cosmic ray and solar particle investigations over the south polar regions of the Sun, *Science, 268*, 1019, 1995.

Smith, E. J., R. G. Marsden, and D. E. Page, Ulysses above the Sun's south pole: An introduction, *Science, 268*, 1005, 1995a.

Smith, E. J., et al., Ulysses observations of latitude gradients in the heliospheric magnetic field: Radial component and variances, *Space Sci. Rev., 72*, 165, 1995b.

Tu, C.–Y., and E. Marsch, A model of solar wind fluctuations with two components: Alfvén waves and convective structures, *J. Geophys. Res., 98*, 1257, 1993.

Tu, C.–Y., and E. Marsch, *MHD Structures, Waves and Turbulence in the Solar Wind: Observations and Theories*, Kluwer Acad. Norwell, Mass., 1995.

Zhou, Y., and W. H. Matthaeus, Transport and turbulence modeling of solar wind fluctuations, *J. Geophys. Res., 95*, 10,291, 1990.

Y. –Q. Lou and R. Rosner, Department of Astronomy and Astrophysics, University of Chicago, Chicago, IL 60637. (e–mail: lou@oddjob.uchicago.edu, rrosner@oddjob.uchicago.edu)

S. Orlando and G. Peres, Istituto ed Osservatorio Astronomico, Piazza del Parlamento 1, 90134 Palermo, Italy. (e–mail: orlando@oapa.astropa.unipa.it; peres@oapa.astropa.unipa.it)

(Received April 15, 1997; revised July 3, 1997; accepted July 9, 1997.)

[1]Istituto ed Osservatorio Astronomico, Palermo, Italy

[2]Department of Astronomy and Astrophysics, University of Chicago, Chicago, Illinois

This preprint was prepared with AGU's LaTeX macros v4. File preprint formatted August 20, 1997.